# Impact of Tank Geometry on the Maximum Turbulence Energy Dissipation Rate for Impellers

**Genwen Zhou and Suzanne M. Kresta**
Dept. of Chemical Engineering, University of Alberta, Edmonton, Alberta, Canada T6G 2G6

*The maximum turbulence energy dissipation rate per unit mass, $\epsilon_{max}$, is an important variable in dispersion systems, particularly for drop breakup and coalescence, and for gas dispersion. The effect of tank geometry (number of baffles, impeller diameter, and off-bottom clearance) on $\epsilon_{max}$ for four impellers (the Rushton turbine, RT; the pitched blade turbine, PBT; the fluidfoil turbine, A310; and the high-efficiency turbine, HE3) is examined. Mean and fluctuating velocity profiles close to the impellers were measured in a cylindrical baffled tank using laser doppler velocimetry. Local and maximum turbulence energy dissipation rates in the impeller region were estimated using $\epsilon = Av^3/L$ with $A = 1$ and $L = D/10$ for all four impellers. Factorial designs were used to test for the effects of single geometric variables under widely varying conditions and interactions between variables. Several factorial designs were used to ensure that real effects were separated from effects that appeared as an artifact of the experimental design. Results show that the tank geometry has a significant effect on $\epsilon_{max}$, primarily with respect to variations in impeller diameter and interactions between the off-bottom clearance and impeller diameter. For the same power input and tank geometry, the RT consistently produces the largest $\epsilon_{max}$ and/or $\epsilon_{max}$ scaled with $N^3D^2$.*

## Introduction

The power input per unit mass of fluid in an agitated tank ($\bar{\epsilon} = P/\rho V_T$) is not sufficient to completely define the characteristics of the turbulence energy dissipation. According to the length scale defined by Kolmogoroff, $\eta = (\nu^3/\epsilon)^{1/4}$, the minimum length scale in a dispersion is determined by the maximum turbulence energy dissipation rate per unit mass, $\epsilon_{max}$, so the *local* turbulence energy dissipation rate is critical. The minimum drop size in a dispersion of gas or liquid will be determined by $\epsilon_{max}$, since all the particles in the dispersion have a finite probability of passing through the position where $\epsilon_{max}$ occurs. Most investigations of drop breakup and gas dispersion, however, characterize $\epsilon_{max}$ by the power input per unit mass $\bar{\epsilon}$, and examine only one tank geometry. Thus, the investigation of the effect of geometry on $\epsilon_{max}$ is important for both improved fundamental understanding and for practical applications.

Since the direct determination of the local turbulence energy dissipation rate $\epsilon$ or $\epsilon_{max}$ by experiments is practically impossible, several methods of estimating the local dissipation have been applied to stirred tanks.

Cutter (1966) started with the Navier–Stokes equations and derived the following equation relating $\epsilon$ to three components of the mean and fluctuating velocities:

$$2\pi r\int_{-\infty}^{+\infty}\epsilon\,dz = \frac{d}{dr}\left[r2\pi\int_0^{\infty}\left(K^2\bar{V}_z + 2\bar{V}_\theta\overline{v'_r v'_\theta}\right)dz\right], \quad (1)$$

where $K^2$ equals $\bar{V}_z^2 + \bar{V}_r^2 + \bar{V}_\theta^2 + v_z^2 + v_r^2 + v_\theta^2$. With Eq. 1 and data for the mean and fluctuating velocities measured by a photographic method in water agitated by a Rushton turbine (RT), Cutter determined the local turbulence energy dissipation. He found that the values of the ratio $\epsilon/\bar{\epsilon}$ vary from 0.25 in the bulk of the tank to 70 in the immediate vicinity of the impeller. This shows a 270-fold difference between local turbulence energy dissipation rates in the tank.

Okamoto et al. (1981) used the integration of the one-dimensional energy spectrum to calculate $\epsilon$. They measured the mean and fluctuating velocities in the flow produced by the RT in both the impeller stream and the bulk of both

Correspondence concerning this article should be addressed to S. M. Kresta.

unbaffled and baffled tanks using a hot-film anemometer. In the unbaffled tank the maximum value of the ratio $\epsilon/\bar{\epsilon}$ was 11.3, near the tip of the impeller, and the minimum value was 0.21, in the bulk of the tank; in the baffled tank the maximum value of the ratio $\epsilon/\bar{\epsilon}$ was 6.50 (near the tip of the impeller) and the minimum value was 0.16 (in the upper region of the tank). The difference between local turbulence energy dissipation rates in this work was 54-fold for the unbaffled case and 41-fold for the baffled case. This indicates that the flow in a baffled tank is less inhomogeneous than the flow in unbaffled tank.

Costes and Couderc (1988) measured the turbulent flow produced by an RT using laser Doppler velocimetry (LDV). They used energy spectrum analysis to determine the local turbulence energy dissipation and found that near the impeller $\epsilon/\bar{\epsilon} \cong 5 \sim 10$, and in the bulk of the tank $\epsilon/\bar{\epsilon} \cong 0.05 \sim 0.07$, values much lower than those reported by Cutter (1966) and Okamoto et al. (1981). The difference between local turbulence energy dissipation rates in the tank was approximately 100-fold.

Wu and Patterson (1989) also measured the turbulent flow produced by an RT using LDV. They used $\epsilon = A(q^{3/2}/L_{res})$ to estimate the local dissipation, in which $q$ is the turbulent kinetic energy and $L_{res}$ is a three-dimensional "resultant" macro length scale. They only reported the values of $\epsilon$ in the impeller stream. The maximum value of the ratio $\epsilon/\bar{\epsilon}$ for their work is about 22 near the tip of the impeller blades.

Considered together, these articles indicate large variations of $\epsilon/\bar{\epsilon}$ throughout the tank, with $\epsilon_{max}$ at least 10 times the average value. There is substantial variation in the reported results, which the results of this article show is partly due to differences in the tank geometries used by the different authors, and partly due to scaling with $\bar{\epsilon}$ instead of with $N^3D^2$ (see Kresta and Wood, 1993a).

No work has been published to date that investigates the effect of tank geometry on the *maximum* turbulence energy dissipation rate in stirred tanks. Research on the effect of tank geometry on the *local* dissipation rate is limited to some very specific correlations reported by Okamoto et al. (1981). They reported the following correlation for the local turbulence energy dissipation rates in the impeller stream $\epsilon_i$, and in the circulation region $\epsilon_c$:

$$\frac{\epsilon_i}{\bar{\epsilon}} = 7.8(D/T)^{-1.38}\exp(-2.46D/T)$$

$$\frac{\epsilon_c}{\bar{\epsilon}} = 0.90(D/T)^{1.10}$$

$$(0.25 \le D/T \le 0.70). \qquad (2)$$

These equations account for the effect of impeller diameter on $\epsilon$. Okamoto et al. (1981) also correlated Sato and coworkers' data to quantify the effects of impeller diameter and of impeller blade width on $\epsilon$:

$$\frac{\epsilon_i}{\bar{\epsilon}} = c_1'(W/T)^{-1.38}\exp(-2.46D/T)$$

$$\frac{\epsilon_c}{\bar{\epsilon}} = c_2'(W/T)^{0.32}(D/T)^{0.78}$$

$$(0.05 \le W/T \le 0.30, \quad 0.25 \le D/T \le 0.70), \qquad (3)$$

where $c_1'$ and $c_2'$ are constants. The value of $c_1'$ was 0.85 for the data with a six-bladed impeller and four baffle plates. The value of $c_2'$ was not given. In fact, Eq. 2 or Eq. 3 can only be used to correlate the effect of the width of impeller blades or impeller diameter on $\epsilon$ for a single point, since the locations of $\epsilon_i$ and $\epsilon_c$ were fixed. Measurements have shown that $\epsilon$ varies from point to point, especially in the region around the impeller blades, so that any single measurement of $\epsilon$ cannot reliably represent the maximum, minimum, or the average dissipation rate in a region. For example, if $D/T = 1/2$, equations give $\epsilon_i = 5.93\bar{\epsilon}$, which is well below the maximum dissipation ($11.3\bar{\epsilon}$) reported by the same authors, and $\epsilon_c = 0.42\bar{\epsilon}$, which is well above the minimum dissipation ($0.16\bar{\epsilon}$) in the upper region of the tank.

This investigation focuses on the effects of one operating variable (rotational speed $N$) and three geometric variables (impeller diameter $D$, off-bottom clearance $C$, and number of baffles $N_f$) on the local rate of turbulence energy dissipation per unit mass, $\epsilon$, close to the impeller. The dissipation was estimated using a simple method based on dimensional analysis and the streamwise root-mean-square (RMS) velocity. Factorial designs and detailed statistical analysis were used to determine the significant geometric variables and interactions. Four impellers were studied: one radial flow impeller (the Rushton turbine (RT)); and three axial flow impellers (the pitched-blade turbine (PBT), the fluidfoil turbine (A310), and the modified pitched-blade turbine (HE3)).

The dimensional method used to estimate the local turbulence energy dissipation for the flow in the impeller region (around the impeller) and in the impeller discharge stream was validated in Zhou and Kresta (1996) and compared with several other methods in Kresta and Wood (1993a). Both articles show good agreement between this simple estimate and other more complex approaches, including those that remove the "pseudoturbulent" component (e.g., Wu and Patterson, 1989). The reader is referred to the original articles for the basis of the method, and the conditions under which it is valid. The equation used for estimating $\epsilon$ was

$$\epsilon = A\frac{v^3}{L}, \qquad (4)$$

with $A = 1$ and $L = D/10$, where $v$ is the streamwise component of fluctuating velocity. For the RT, $v$ is the radial RMS velocity in the impeller discharge stream at the tip of impeller blades, while for the PBT, A310, and HE3, $v$ is the axial RMS velocity below the blades.

The effect of tank geometry on the maximum dissipation was investigated using factorial designs of experiments. Factorial designs are ideally suited to initial investigations such as this one, where it is not initially clear which variables will be important. They are based on the premise that not only single variables may be important, but variables may interact to produce magnified, or opposite, effects. Thus, an experimental block based on a factorial design can give a more general picture of the phenomenon of interest with a limited number of experiments. However, because the data are limited, a very careful analysis of the results is required. The variables must be chosen carefully if they are to reflect the underlying physics, and the initial experimental design must

often be modified and expanded to check conclusions, and to test hypotheses obtained from the initial results. For this study, three factorial designs were evolved, and the results were analyzed using a combination of 95% confidence intervals, normal probability plots, and a detailed examination of the data.

## Experimental Studies

### *LDA*

A one-dimensional LDV was used in this study. Two beams from an argon-ion laser passed the transmitting and focusing optics to intersect and form a measuring volume within a cylindrical, baffled tank, immersed in a square tank filled with water to minimize optical distortion. All walls of both tanks were made from Perspex. The two tanks were moved horizontally using computer-controlled traverses, and vertically using a manual traverse. The rotational speed of the impeller was measured using an optical tachometer. The receiving optics were operated in a forward-scattering mode.

An Aerometrics Doppler signal analyzer (DSA) was used to convert analog signals from the receiving optics into Doppler frequencies and velocities. The DSA uses frequency-domain burst detection to convert the analog signal into instantaneous velocity measurements. The analog signal was sampled at a rate between 2.5 and 10 MHz. Comparison of the velocity measurements from three separate detectors, based on this signal sampling rate, gave a data validation rate $\geq 99\%$.

For signal analysis based on burst detection, the frequency of velocity measurement is closely tied to the particle arrival rate, or the seeding density. For these experiments, the average frequency of velocity measurement was 1.2 kHz. Note that since only time-averaged velocities are of interest here, the velocity sampling rate does not affect the results and is provided only for information. A sample size of 6,000 instantaneous velocity determinations was needed to give good reproducibility of the mean and RMS velocities. Comparison of the results with those obtained using a counterprocessor (Kresta and Wood, 1993b) showed no measurable velocity bias.

### *Geometry of the baffled tank and the impellers*

The baffled tank is shown in Figure 1. Four vertical baffles (width = $T/10$) were equally spaced around the periphery of the tank. The liquid depth, $H$, was equal to the tank diameter ($H = T$). The off-bottom clearance, $C$, is defined as the distance between the bottom of the tank and the *center line* of the impeller blades. The origin of the cylindrical coordinates is defined as the crosspoint of the shaft axis and the line from a baffle to a baffle at the centerline of the impeller blades. To prevent vortexing and the entry of air into the system, a lid was installed on top of the baffles, and covered with 5 cm of water to seal the tank. This had no observable effect on the measured velocities in the impeller region.

All four impellers were used in their standard configurations. The four-bladed PBT had blades inclined at 45° to the horizontal; the blade width of the PBT and RT was $D/5$; the blade length of the RT was $D/4$; and the disk diameter of the RT was $2/3D$. The A310 was used as supplied by Lightnin' Inc., and the HE3 was used as supplied by Chemineer.

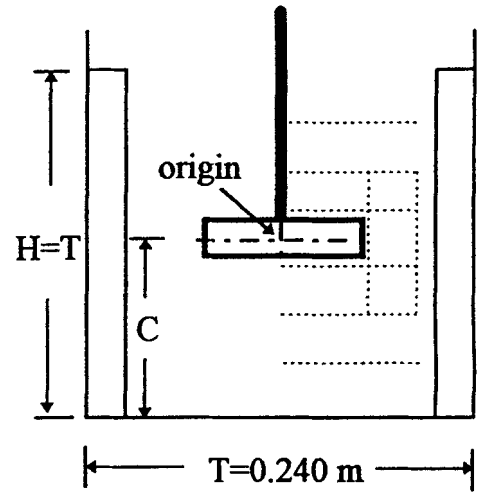


**Figure 1. Stirred tank and the measuring traverses (····) used to locate $\epsilon_{max}$ for each of the four impellers.**

### *Experimental designs*

All of the experimental runs and experimental results are summarized in Tables 1–4. For each impeller, three sets of experiments were run. The first was used to verify the scaling of $\epsilon$ with $N^3$. The second was a factorial design in $N_f$, $D$, and $C$. The third was a modified factorial design using the dimensionless off-bottom clearance $C/D$, instead of $C$.

*Rotational Speed.* To test the effect of rotational speed on $\epsilon_{max}$, five different $N$'s ($N1$ to $N5$ in Tables 1 to 4) were used in the same tank geometry for each of the four impellers. One rotational speed (bold in Tables 1 to 4) was chosen to match the power input used in the factorial designs.

*Factorial Design in $N_f$, $D$, and $C$.* To examine the effects of the three geometric variables on $\epsilon_{max}$, factorial designs with three variables at two levels (designated $+1$ and $-1$) were applied.

The number of baffles, $N_f$, and impeller diameter, $D$, are two of the most important geometric variables in the study of mixing. Two alternatives are used in the literature for the off-bottom clearance: $C$ or $C/D$. For the first factorial design, $C$ was chosen as a geometric variable. Thus the first set of experiments used the three geometric variables $N_f$, $D$, and $C$ (Runs 1 to 8 in Tables 1 to 4). $N_f$ is either 4 ($+1$) or 2 ($-1$); $D$ is either $T/2$ ($+1$) or $T/4$ ($-1$); and $C$ is either $T/2$ ($+1$) or $T/4$ ($-1$).

*Factorial Design in $N_f$, $D$, and $C/D$.* Analysis of the experimental data in the first factorial design indicated that a modified design was needed. This modified design was then carried out with the variables $N_f$, $D$, and $C/D$ (Runs 3 to 10 in Tables 1 to 4). When $C/D$ was chosen as a geometric variable, $C/D$ was either 1 ($+1$) or 0.5 ($-1$).

In summary, there are two sets of experiments for factorial designs: the first is based on $N_f$, $D$, and $C$; the second on $N_f$, $D$, and $C/D$. Each has three variables at two levels. The number of experimental runs for each factorial design is 8: $2\times2\times2$. In the third factorial design, the second set of data was rescaled from constant power input ($N^3D^5$ = constant), to constant dissipation ($N^3D^2$ = constant) and reanalyzed.

Table 1. Experimental Design and Results: PBT

| Run | $N_f$ +4 −2 | $D$ +T/2 0 T/3 −T/4 | $C$ +T/2 0 T/3 −T/4 | C/D +1 −1/2 | N rpm | Re *10⁻⁴ | $\bar{\epsilon}$ m²/s³ | $\epsilon_{max}$ m²/s³ | $\epsilon_{max}/N^3D^2$ |
|---|---|---|---|---|---|---|---|---|---|
| 1 | + | − | + | | 1,133 | 6.69 | 0.652 | 51.5 | 2.13 |
| 2 | − | − | + | | 1,133 | 6.69 | 0.652 | 56.2 | 2.32 |
| 3 | + | − | − | + | 1,133 | 6.69 | 0.652 | 43.2 | 1.78 |
| 4 | − | − | − | + | 1,133 | 6.69 | 0.652 | 48.2 | 1.99 |
| 5 | + | + | + | + | 357 | 8.43 | 0.652 | 12.0 | 3.94 |
| 6 | − | + | + | + | 357 | 8.43 | 0.652 | 10.5 | 3.47 |
| 7 | + | + | − | − | 357 | 8.43 | 0.652 | 10.1 | 3.32 |
| 8 | − | + | − | − | 357 | 8.43 | 0.652 | 9.46 | 3.12 |
| 9 | + | − | | − | 1,133 | 6.69 | 0.652 | 77.6 | 3.20 |
| 10 | − | − | | − | 1,133 | 6.69 | 0.652 | 69.1 | 2.85 |
| Varying Rotational Speed | | | | | | | | | |
| *N*-1 | + | 0 | 0 | | 357 | 3.75 | 0.086 | 3.34 | 2.47 |
| *N*-2 | + | 0 | 0 | | 480 | 5.04 | 0.209 | 7.71 | 2.36 |
| *N*-3 | + | 0 | 0 | | 580 | 6.09 | 0.368 | 15.1 | 2.62 |
| ***N*-4** | + | **0** | **0** | | **701** | **7.36** | **0.652** | **23.8** | **2.33** |
| *N*-5 | + | 0 | 0 | | 800 | 8.40 | 0.966 | 37.1 | 2.44 |

For each of the experimental runs, Tables 1 to 4 list the combinations of variables, the values of the Reynolds number, the power input per unit mass $\bar{\epsilon}$, $\epsilon_{max}$, and $\epsilon_{max}$ made dimensionless with $N^3D^2$. Scaling of the local dissipation with $N^3D^2$ is based on the fact that $\epsilon$ is proportional to $v^3/D$ (from reduction of the time-averaged equations of turbulence (Kresta and Wood, 1991)) and $v \propto ND$, so $\epsilon$ is proportional to $N^3D^2$.

The power input used for calculating $\bar{\epsilon}$ was computed using the power number ($N_p$) for each impeller. For the tank geometries used in this study, the power numbers for the four impellers are: 5.4 for the RT; 1.35 for the PBT; 0.30 for the A310; 0.25 for the HE3 with $D/T = 1/2$; and 0.30 for the HE3 with $D/T = 1/4$. The power numbers for the HE3 were supplied by Chemineer Inc.; the power number for the A310 was supplied by Lightnin'; and the power numbers for the PBT and the RT were averaged from data published by previous investigators.

## Results

### *Determination of the location of the maximum dissipation*

According to Eq. 4, $\epsilon_{max}$ appears at the same position as the maximum fluctuating velocity. In order to avoid locating the position of $\epsilon_{max}$ arbitrarily, all three fluctuating velocities were measured on traverses in both the impeller regions and the bulk of the tank (Figure 1). The radial traverse just below and just above the impeller blades are both 2 mm away from the impeller blades. The axial traverse near the tip of impeller blades is 3 mm away from the impeller tip. From these measurements, several conclusions were drawn.

The maximum fluctuating velocity is $v_z$ for the three axial flow impellers (the PBT, A310, and HE3), and it always occurs just below the impeller blades. Figures 2a and 2b show radial profiles of $v_z$ for the PBT and A310, respectively. The line with $z = -10.5$ mm in Figure 2a represents the radial traverse 2 mm below the impeller blades (the projected blade

Table 2. Experimental Design and Results: A310

| Run | $N_f$ +4 −2 | $D$ +0.550T 0 0.475T −0.350T | $C$ +T/2 0 T/3 −T/4 | C/D +1 −1/2 | N rpm | Re *10⁻⁴ | $\bar{\epsilon}$ m²/s³ | $\epsilon_{max}$ m²/s³ | $\epsilon_{max}/N^3D^2$ |
|---|---|---|---|---|---|---|---|---|---|
| 1 | + | − | + | | 1,068 | 12.4 | 0.652 | 30.2 | 0.758 |
| 2 | − | − | + | | 1,068 | 12.4 | 0.652 | 28.1 | 0.706 |
| 3 | + | − | − | + | 1,068. | 12.4 | 0.652 | 25.9 | 0.652 |
| 4 | − | − | − | + | 1,068. | 12.4 | 0.652 | 20.9 | 0.526 |
| 5 | + | + | + | + | 503 | 14.4 | 0.652 | 12.5 | 1.22 |
| 6 | − | + | + | + | 503 | 14.4 | 0.652 | 11.6 | 1.13 |
| 7 | + | + | − | − | 503 | 14.4 | 0.652 | 8.43 | 0.821 |
| 8 | − | + | − | − | 503 | 14.4 | 0.652 | 8.16 | 0.795 |
| 9 | + | − | | − | 1,068 | 12.4 | 0.652 | 26.1 | 0.655 |
| 10 | − | − | | − | 1,068 | 12.4 | 0.652 | 18.6 | 0.467 |
| Varying Rotational Speed | | | | | | | | | |
| *N*-1 | + | 0 | 0 | | 430 | 9.17 | 0.196 | 4.69 | 0.979 |
| *N*-2 | + | 0 | 0 | | 503 | 10.7 | 0.313 | 7.36 | 0.961 |
| *N*-3 | + | 0 | 0 | | 570 | 12.2 | 0.456 | 10.9 | 0.976 |
| ***N*-4** | + | **0** | **0** | | **642** | **13.7** | **0.652** | **15.2** | ***0.952*** |
| *N*-5 | + | 0 | 0 | | 720 | 15.3 | 0.919 | 21.7 | 0.967 |

**Table 3. Experimental Design and Results: HE3**

| Run | $N_f$ +4 −2 | $D$ +T/2 0 T/3 − T/4 | $C$ + T/2 0 T/3 − T/4 | $C/D$ +1 − 1/2 | $N$ rpm | $Re$ *10$^{-4}$ | $\bar{\epsilon}$ m$^2$/s$^3$ | $\epsilon_{max}$ m$^2$/s$^3$ | $\frac{\epsilon_{max}}{N^3D^2}$ |
|---|---|---|---|---|---|---|---|---|---|
| 1 | + | − | + | | 1,694 | 10.0 | 0.484 | 70.6 | 0.871 |
| 2 | − | − | + | | 1,694 | 10.0 | 0.484 | 86.8 | 1.07 |
| 3 | + | − | − | + | 1,694 | 10.0 | 0.484 | 65.6 | 0.810 |
| 4 | − | − | − | + | 1,694 | 10.0 | 0.484 | 80.7 | 0.996 |
| 5 | + | + | + | + | 567 | 13.4 | 0.484 | 13.1 | 1.08 |
| 6 | − | + | + | + | 567 | 13.4 | 0.484 | 15.1 | 1.24 |
| 7 | + | + | − | − | 567 | 13.4 | 0.484 | 6.73 | 0.554 |
| 8 | − | + | − | − | 567 | 13.4 | 0.484 | 7.53 | 0.620 |
| 9 | + | − | | − | 1,694 | 10.0 | 0.484 | 59.2 | 0.731 |
| 10 | − | − | | − | 1,694 | 10.0 | 0.484 | 53.8 | 0.664 |
| | | | Varying Rotational Speed | | | | | | |
| *N*-1 | + | 0 | 0 | | 861 | 9.04 | 0.259 | 24.4 | 1.29 |
| *N*-2 | + | 0 | 0 | | 961 | 10.1 | 0.360 | 35.2 | 1.34 |
| ***N*-3** | + | **0** | **0** | | **1,061** | **11.1** | **0.484** | **48.1** | **1.36** |
| *N*-4 | + | 0 | 0 | | 1,161 | 12.2 | 0.634 | 58.7 | 1.27 |
| *N*-5 | + | 0 | 0 | | 1,261 | 13.2 | 0.812 | 74.3 | 1.25 |

width, $W_p$, is 17.0 mm, half of $W_p$ is 8.5 mm) and the maximum $v_z$ always appears on this traverse. The same is true for the A310, but note that two clear peaks occur on the traverse where the maximum $v_z$ appears. Experimental results showed that for axial flow impellers the maximum fluctuating velocity is the axial fluctuating velocity for all 15 runs examined, although in the impeller region, the radial and tangential fluctuating velocities are nearly the same as the axial fluctuating velocity (Zhou and Kresta, 1996).

For the radial flow impeller (RT), the maximum $v_r$ always appears at the tip of impeller blades, and the maximum fluctuating velocity is $v_r$ (with the exception of run 3, where the maximum component was $v_z$). In this article only the effects of geometric variables on the maximum dissipation calculated with the radial fluctuating velocity are considered. Figure 2c shows the axial profiles of $v_r$ for the RT at the two radii of 63 mm and 87 mm. From Figure 2c, the maximum $v_r$ appears at $r = 63$ mm, but the profiles of $v_r$ decay slowly in the impeller discharge stream. Thus the maximum turbulence energy dissipation is approximately constant in this region.

As stated earlier, the work reported in this article is primarily an investigation of the effect of geometry on $\epsilon_{max}$. To be sure that the location of the traverse containing $\epsilon_{max}$ is independent of geometry, the effect of geometry on the location of this traverse was investigated. It was found that the traverse on which $\epsilon_{max}$ is found is independent of clearance, impeller diameter, and number of baffles.

With the locations of the maximum fluctuating velocities and thus $\epsilon_{max}$ determined, streamwise velocity measurements were performed on a single traverse to find $\epsilon_{max}$. For the PBT, A310, and HE3, the axial fluctuating velocity was measured on a radial traverse 2 mm below the impeller blades; for the RT, the radial fluctuating velocity was measured on an axial traverse 3 mm away from the tip of the RT blades.

**Table 4. Experimental Design and Results: RT**

| Run | $N_f$ +4 − 2 | $D$ + T/2 0 T/3 − T/4 | $C$ + T/2 0 T/3 − T/4 | $C/D$ +1 − 1/2 | $N$ rpm | $Re$ *10$^{-4}$ | $\bar{\epsilon}$ m$^2$/s$^3$ | $\epsilon_{max}$ m$^2$/s$^3$ | $\frac{\epsilon_{max}}{N^3D^2}$ |
|---|---|---|---|---|---|---|---|---|---|
| 1 | + | − | + | | 714 | 4.22 | 0.652 | 59.1 | 9.75 |
| 2 | − | − | + | | 714 | 4.22 | 0.652 | 81.7 | 13.5 |
| 3 | + | − | − | + | 714 | 4.22 | 0.652 | 89.8 | 14.8 |
| 4 | − | − | − | + | 714 | 4.22 | 0.652 | 84.3 | 13.9 |
| 5 | + | + | + | + | 225 | 5.31 | 0.652 | 13.5 | 17.1 |
| 6 | − | + | + | + | 225 | 5.31 | 0.652 | 9.42 | 12.4 |
| 7 | + | + | − | − | 225 | 5.31 | 0.652 | 15.1 | 19.9 |
| 8 | − | + | − | − | 225 | 5.31 | 0.652 | 13.8 | 18.1 |
| 9 | + | − | | − | 714 | 4.22 | 0.652 | 74.6 | 12.3 |
| 10 | − | − | | − | 714 | 4.22 | 0.652 | 74.6 | 12.3 |
| | | | Varying Rotational Speed | | | | | | |
| *N*-1 | + | 0 | 0 | | 225 | 2.36 | 0.086 | 4.10 | 12.1 |
| *N*-2 | + | 0 | 0 | | 300 | 3.15 | 0.204 | 9.73 | 12.2 |
| *N*-3 | + | 0 | 0 | | 370 | 3.88 | 0.382 | 17.8 | 11.8 |
| ***N*-4** | + | **0** | **0** | | **442** | **4.64** | **0.652** | **31.4** | **12.3** |
| *N*-5 | + | 0 | 0 | | 510 | 5.35 | 1.00 | 48.4 | 12.3 |

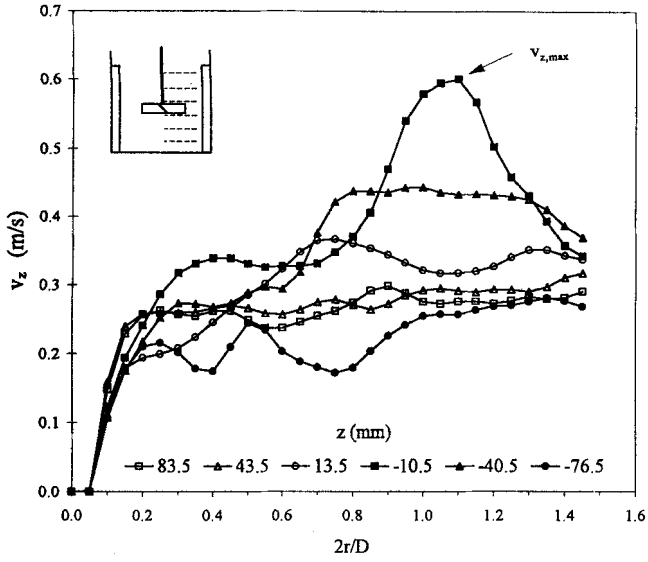


(a)

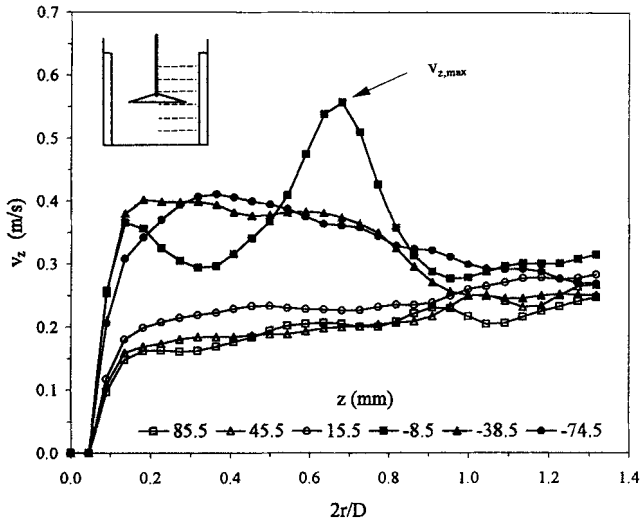


(b)

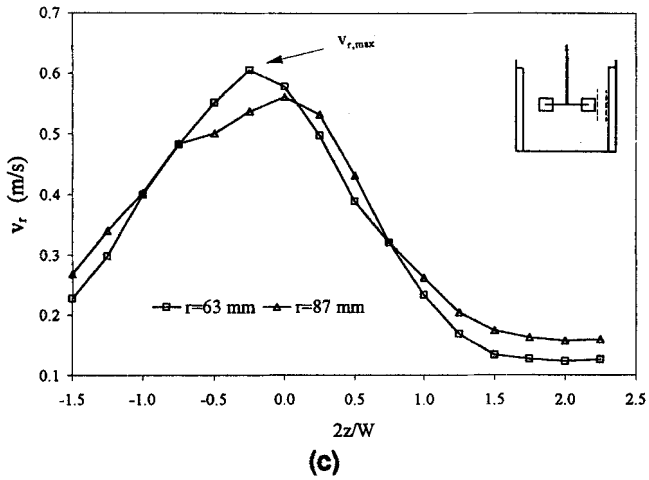


(c)

**Figure 2. Velocity profiles used to locate $\epsilon_{max}$.**

(a) PBT; radial profiles of $v_z$; $N_f = 4$, $D = T/2$, $C = T/3$, $N = 400$ rpm. (b) A310; radial profiles of $v_z$; $N_f = 4$, $D = 0.550T$, $C = T/3$, $N = 652$ rpm. (c) RT; axial profiles of $v_r$; $N_f = 4$, $D = T/2$, $C = T/3$, $N = 221$ rpm.

The velocity was measured at 3-mm intervals. In the figures that follow, the dimensionless variables ($2r/D$ and $2z/W$) are used.

### *Effect of rotational speed on* $\epsilon_{max}$

If the flow is fully turbulent, the fluctuating velocities scale exactly with the tip speed of an impeller for a constant tank geometry. Thus, from Eq. 4, $\epsilon$ should be proportional to $N^3$. This is supported by the experimental results of this work. Profiles of the scaled $\epsilon$ for five different $N$'s are shown in Figures 3a to 3d for the PBT, A310, HE3, and RT, respectively. The five profiles of the scaled $\epsilon$ overlap in all four figures, as do the five scaled $\epsilon_{max}$. Note that this close agreement appears even though the experimental error in the velocity measurements has been cubed. These results confirm that $\epsilon_{max}$ is proportional to $N^3$ *when the geometry and scale are constant.* Two peaks are clearly shown for the A310. Experimental results show that this double peak appears consistently for the A310, regardless of the geometry used.

### *Range of variation in scaled* $\epsilon_{max}$

Different impellers create different flow fields. It is important to know how the impeller style and tank geometry affect $\epsilon_{max}$ because of its importance in determining process results. Figure 4 compares the scaled $\epsilon_{max}$ for all 60 experiments. The RT runs were arranged in order of increasing values of the scaled $\epsilon_{max}$. Runs for the PBT, A310, and HE3 were arranged to match the RT geometry. Serial numbers 2–6 on each of the four lines represent the five runs with different rotational speeds and the same geometry.

The values of the scaled $\epsilon_{max}$ for the RT, ranging from 9.75 to 19.9, are much larger than for the three axial flow impellers, none of which exceed 4. The values of the scaled $\epsilon_{max}$ for the A310 and the HE3 follow each other closely over changes in tank geometry. The magnitude of the scaled $\epsilon_{max}$ shows the same trend as the power number: the impellers with larger power numbers generate larger scaled $\epsilon_{max}$. This is to be expected, since $N$ was set for each run based on a constant power input.

### *Effect of tank geometry on* $\epsilon_{max}$

The experimental runs designed to study the effect of tank geometry on $\epsilon_{max}$ were based on three factorial designs for each of the four impellers. These experiments are summarized in Tables 1 to 4. For each set of experiments, there are three main variables ($N_f$, $D$, and $C$ or $C/D$) and four possible interactions between these variables ($N_f-D$, $N_f-C$, $D-C$, and $N_f-D-C$; or $N_f-D$, $N_f-C/D$, $D-C/D$, and $N_f-D-C/D$); therefore there are seven possible geometric effects.

Effects of these geometric variables on $\epsilon_{max}$ are estimated using the method of Box et al. (1978). Factorial designs will not be reviewed in detail here, but the method of calculating the effects of variables is explained. By denoting two levels of each variable with $+1$ representing the higher level and $-1$ representing the lower level, the effect of a variable on $\epsilon_{max}$ scaled with $N^3D^2$ (namely, $\epsilon_{max,scaled}$ in the equation below) can be calculated using the following expression:

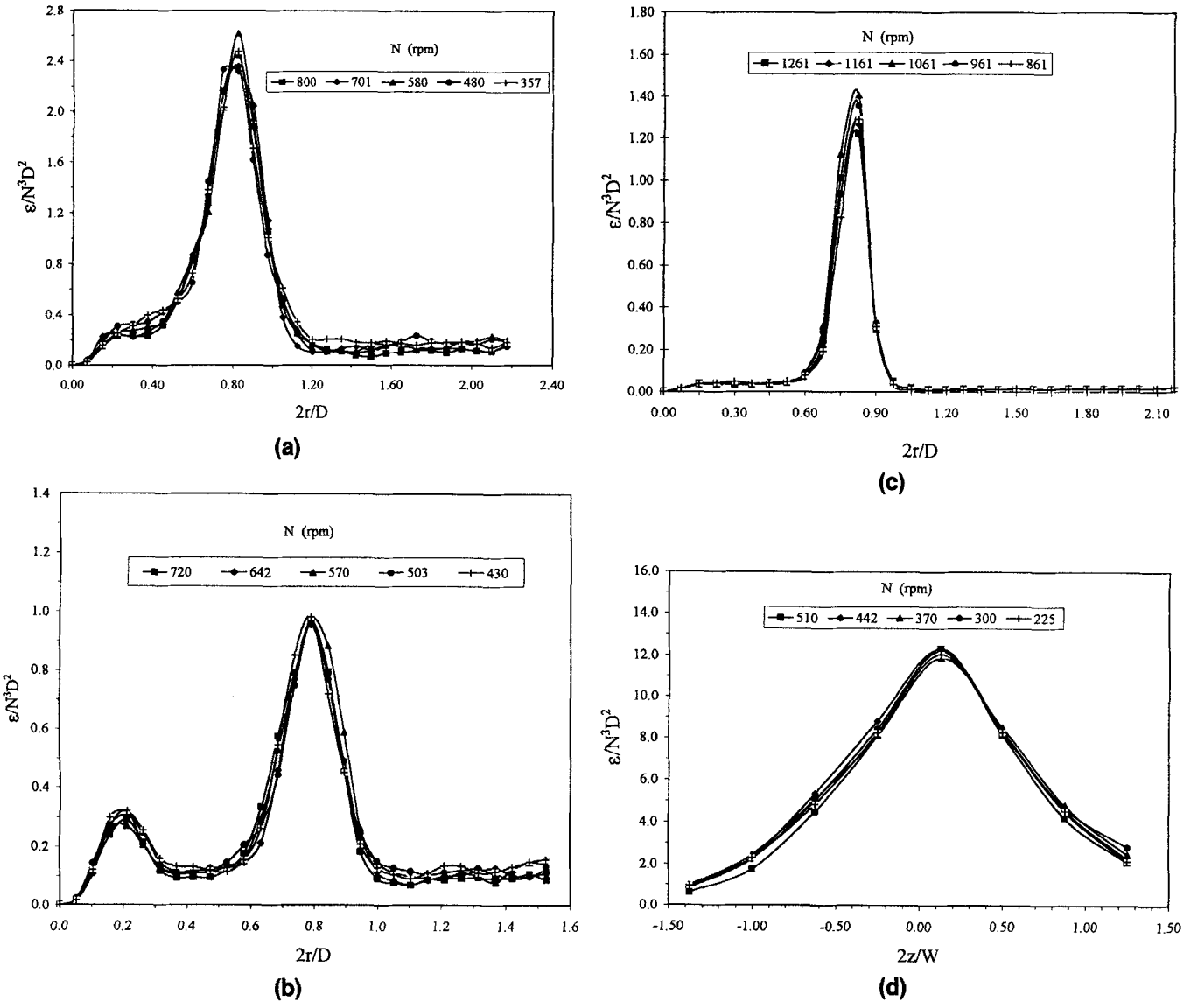


**Figure 3. Validation of the scaling of $\epsilon$ with $N^3$; $N_f = 4$, $C = T/3$.**

(a) PBT; $D = T/3$, $2z/W_p = -1.35$. (b) A310; $D = 0.475T$, $2z/W_p = -1.30$. (c) HE3; $D = T/3$, $2z/W_p = -1.46$. (d) RT; $D = T/3$, $2r/D = 1.08$.

$$e_i = \frac{\Sigma l_i \epsilon_{\max,\text{scaled}}}{4}, \tag{5}$$

where $\Sigma$ means to take the sum of all eight runs, and $l_i$ is the product of the levels for variable or interaction $i$. For example, in run 1 for the first factorial design in Tables 1 to 4, the number of baffles, $N_f$ (variable 1), and the off-bottom clearance, $C$ (variable 3), were both at the $+1$ level; the impeller diameter, $D$ (variable 2), was at the $-1$ level. Thus the levels of the main effects for $N_f$, $C$, and $D$ are $+1$, $+1$, and $-1$, respectively; the level of the interaction between $N_f$–$C$, $l_{13}$, is $+1$. Similarly, $l_{12}$, $l_{23}$, and $l_{123}$ are all $-1$. $\epsilon_{\max,\text{scaled}}$ is the scaled $\epsilon_{\max}$ of the corresponding run. In this way, the three main effects and the four interactions were calculated one by one. The method used to calculate the geometric effects on $\epsilon_{\max}$ was similar. The results are summarized in Tables 5, 6 and 7.

Note that all experiments in the three factorial designs have a constant power input per unit mass. $\bar{\epsilon}$ was 0.652 $m^2/s^3$ for the PBT, A310, and RT, while $\bar{\epsilon}$ was 0.484 $m^2/s^3$ for the HE3. The HE3 $\bar{\epsilon}$ was lower than the $\bar{\epsilon}$ used for the PBT, A310, and RT due to limitations on the rotational speed set by operational stability and prevention of the suction of air bubbles. Because the scaling with $N^3$ was shown to be exact, this difference in experimental conditions did not preclude comparisons between impellers.

### *Criteria used to evaluate the statistical significance of the effects*

The effect of a variable on $\epsilon_{\max}$ can either be a true effect resulting from the variable, or can be caused by chance occurrences. It is necessary to analyze the statistical significance of the geometric effects on $\epsilon_{\max}$ to distinguish whether

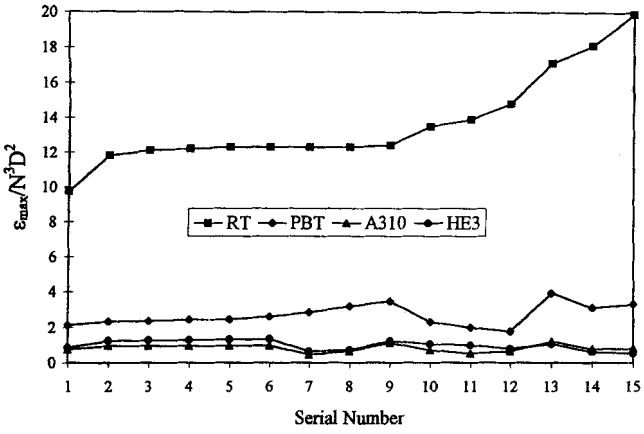


**Figure 4. Comparison of the scaled $\epsilon_{max}$ for all experiments.**

The RT data were arranged in the order of increasing $\epsilon_{max}/N^3D^2$. Runs for the PBT, A310, and HE3 were arranged to match the RT geometry with the same serial number.

the effects are caused by chance occurrences or are real effects. Three criteria were used to assess the significance of effects: the 95% confidence interval (or estimated experimental error), normal probability plots, and a detailed evaluation of the data.

*Ninety-five Percent Confidence Interval, or Estimated Experimental Error.* The effects of geometric variables on $\epsilon_{max}$ may be partly attributed to experimental errors in the velocity measurements. Separation of the real effects from the experimental errors is critical to accurate statistical analysis. The experimental errors were quantified by a 95% confidence interval using the data at five different rotational speeds and the same geometry (runs $N1$ to $N5$). Given that the five scaled $\epsilon_{max}$ for five different rotational speeds with the same geometry should be equal, the differences between them may be attributed to experimental errors. Thus the mean value of the five scaled $\epsilon_{max}$ and the sample standard deviation can be computed for each of the four impellers. The 95% confidence interval (95% C.I.) for each of the impellers was determined by assuming a $t$-distribution with four degrees of freedom. The calculated results are listed in the upper portion of Table 8. Effects that fall outside the 95% C.I. cannot be attributed entirely to experimental error. Note that the A310 impeller produces a more stable flow field and its velocity measurement has a correspondingly good reproducibility. This is reflected by an extremely small standard deviation.

*Normal Probability Plots.* When the calculated effects given in Tables 5 and 6 are plotted on normal probability plots, the effects that are randomly distributed are expected to fall on a straight line. Box et al. (1978) state that if the seven effects (main effects and interactions) occur simply as the result of random variation about a fixed mean, and the changes in levels of the variables have no real effect on the scaled $\epsilon_{max}$, *then the seven effects are roughly normal and distributed about zero.* Thus, when normal probability plots are used, effects that do not fall on a straight line may be considered significant.

*Detailed Evaluation of Experimental Data.* Using the 95% C.I. and normal probability plots as guides, the differences between experimental runs were evaluated in detail. This last

**Table 5. Calculated Effects of Geometric Variables and Interactions on $\epsilon_{max}/N^3D^2$ for the Factorial Design Based on $N_f$, $D$, and $C$***

| Variable or Interaction | Effect on the Scaled $\epsilon_{max}$ | | | |
|---|---|---|---|---|
| Impeller | PBT | A310 | HE3 | RT |
| $N_p$ | 1.35 | 0.30 | 0.25 ~ 0.30 | 5.4 |
| Power input per unit mass | 0.652 | 0.652 | 0.484 | 0.652 |
| Average of $\epsilon_{max}/N^3D^2$ | 2.78 | 0.826 | 0.906 | 14.9 |
| Main effects | | | | |
| Number of baffles, $N_f$ | 0.0350 | 0.0735 | −0.154 | 0.963 |
| Impeller diameter, $D$ | 1.38 | 0.331 | −0.0623 | 3.84 |
| Clearance, $C$ | 0.445 | 0.255 | 0.321 | −3.54 |
| Two-factor interactions | | | | |
| $N_f \times D$ | 0.300 | −0.0155 | 0.0383 | 2.39 |
| $N_f \times C$ | 0.0400 | −0.00250 | −0.0283 | −0.388 |
| $D \times C$ | 0.0400 | 0.112 | 0.254 | −0.813 |
| Three-factor interaction | | | | |
| $N_f \times D \times C$ | 0.095 | 0.0345 | −0.0218 | **1.94** |

*Scaling of $N$ for constant power input.

**Table 6. Calculated Effects of Geometric Variables and Interactions on $\epsilon_{max}/N^3D^2$ for the Factorial Design Based on $N_f$, $D$, and $C/D$***

| Variable or Interaction | Effect on the Scaled $\epsilon_{max}$ | | | |
|---|---|---|---|---|
| Impeller | PBT | A310 | HE3 | RT |
| $N_p$ | 1.35 | 0.30 | 0.25 ~ 0.30 | 5.4 |
| Power input per unit mass | 0.652 | 0.652 | 0.484 | 0.652 |
| Average of $\epsilon_{max}/N^3D^2$ | 2.96 | 0.783 | 0.837 | 15.1 |
| Main effects | | | | |
| Number of baffles, $N_f$ | 0.202 | 0.108 | −0.088 | 1.87 |
| Impeller diameter, $D$ | 1.01 | 0.417 | 0.074 | 3.58 |
| Ratio of clearance to diameter, $C/D$ | −0.328 | 0.198 | 0.390 | −1.08 |
| Two-factor interactions | | | | |
| $N_f \times D$ | 0.133 | −0.050 | −0.028 | 1.38 |
| $N_f \times C/D$ | −0.072 | −0.001 | −0.087 | −0.925 |
| $D \times C/D$ | 0.813 | 0.170 | 0.185 | −3.18 |
| Three-factor interaction | | | | |
| $N_f \times D \times C/D$ | 0.208 | 0.020 | −0.038 | 0.525 |

*Scaling of $N$ for constant power input.

**Table 7. Calculated Effects of Geometric Variables and Interactions on $\epsilon_{max}$ for the Factorial Design Based on $N_f$, and $D$, and $C/D$***

| Variable or Interaction | Effect on $\epsilon_{max}$ | | | |
|---|---|---|---|---|
| Impeller | PBT | A310 | HE3 | RT |
| $N_p$ | 1.35 | 0.30 | 0.25 ~ 0.30 | 5.4 |
| Power input per unit mass | 0.652 | 0.652 | 0.652 | 0.652 |
| Average of $\epsilon_{max}$ | 8.97 | 8.04 | 12.6 | 11.4 |
| Main effects | | | | |
| Number of baffles, $N_f$ | 0.614 | 1.10 | −1.36 | 1.42 |
| Impeller diameter, $D$ | 3.06 | 4.28 | 3.40 | 2.73 |
| Ratio of clearance to diameter, $C/D$ | −0.992 | 2.03 | 6.11 | −0.817 |
| Two-factor interactions | | | | |
| $N_f \times D$ | 0.402 | −0.507 | −0.544 | 1.04 |
| $N_f \times C/D$ | −0.219 | 0.005 | −1.27 | −0.702 |
| $D \times C/D$ | 2.463 | 1.74 | 3.31 | −2.41 |
| Three-factor interaction | | | | |
| $N_f \times D \times C/D$ | 0.629 | 0.323 | −0.454 | 0.399 |

*$\epsilon_{max}$ for the 16 cases with small $D$ were divided by $(D_1/D_2)^3$ to give scaling for constant $\epsilon_{max}$.

**Table 8. Ninety-five Percent Confidence Intervals Calculated from $\epsilon_{max}/N^3D^2$ Values for the Five Runs with Varying $N$**

| Impeller | Mean | Std. Dev. | 95% C.I. |
|---|---|---|---|
| PBT | 2.44 | 0.114 | 0.316 |
| A310 | 0.967 | 0.011 | 0.031 |
| HE3 | 1.30 | 0.047 | 0.133 |
| RT | 12.1 | 0.207 | 0.575 |

**Ninety-five Percent Confidence Intervals Calculated from $\epsilon_{max}$ Values for the Five Runs with Varying $N$**

| Impeller | Mean | Std. Dev. | 95% C.I. |
|---|---|---|---|
| PBT | 7.41 | 0.345 | 0.957 |
| A310 | 9.93 | 0.113 | 0.314 |
| HE3 | 15.8 | 0.577 | 1.60 |
| RT | 9.22 | 0.157 | 0.437 |

step is crucial for determining the physical meaning behind the statistical analysis, and for evaluating the validity of the experimental design.

In the final analysis, only effects that meet all three criteria can be considered significant.

### *Discussion of significant effects*

Three factorial designs are discussed here: the first is based on the variables $N_f$, $D$, and $C$ with constant power input or $\bar{\epsilon}$; the second on $N_f$, $D$, and $C/D$, again with constant power input; and the third on the $N_f$, $D$, and $C/D$ design rescaled to a basis of constant $\epsilon_{max}$. While some significant differences are apparent between the first and second factorial designs, none appear between the second and third when the results are rescaled. The conclusions drawn are based not only on the statistical analysis, but on the overall behavior of the flow field, and on the combined results of the three factorial designs.

*First Factorial Design: $N_f$, D, and C, Scaling Based on Constant $P/V_T$.* The 95% confidence intervals and normal probability plots for the first factorial design are shown in Figures 5a to 5d. Figures 6a to 6d show the full details of all eight experimental traverses for each of the four impellers. To aid the interpretation of these figures, the runs are grouped into two sets of four based on impeller diameter. Symbols of the same shape are used for the same off-bottom clearance, with

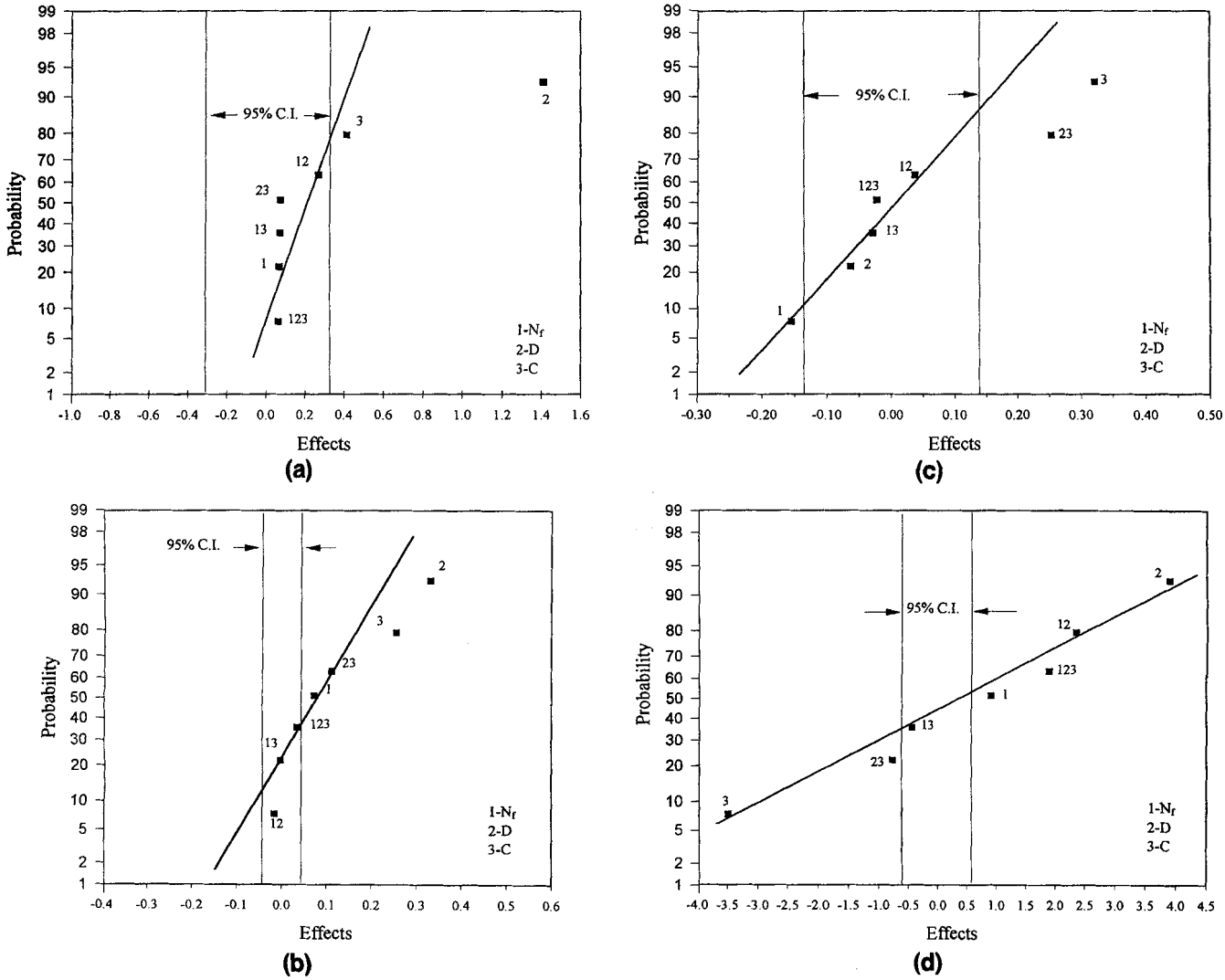


**Figure 5. Normal probability plots of the effects of geometric variables on $\epsilon_{max}/N^3D^2$ showing the 95% confidence interval around zero effect for the factorial design based on $N_f$, $D$, and $C$.**

(a) PBT; (b) A310; (c) HE3; (d) RT.

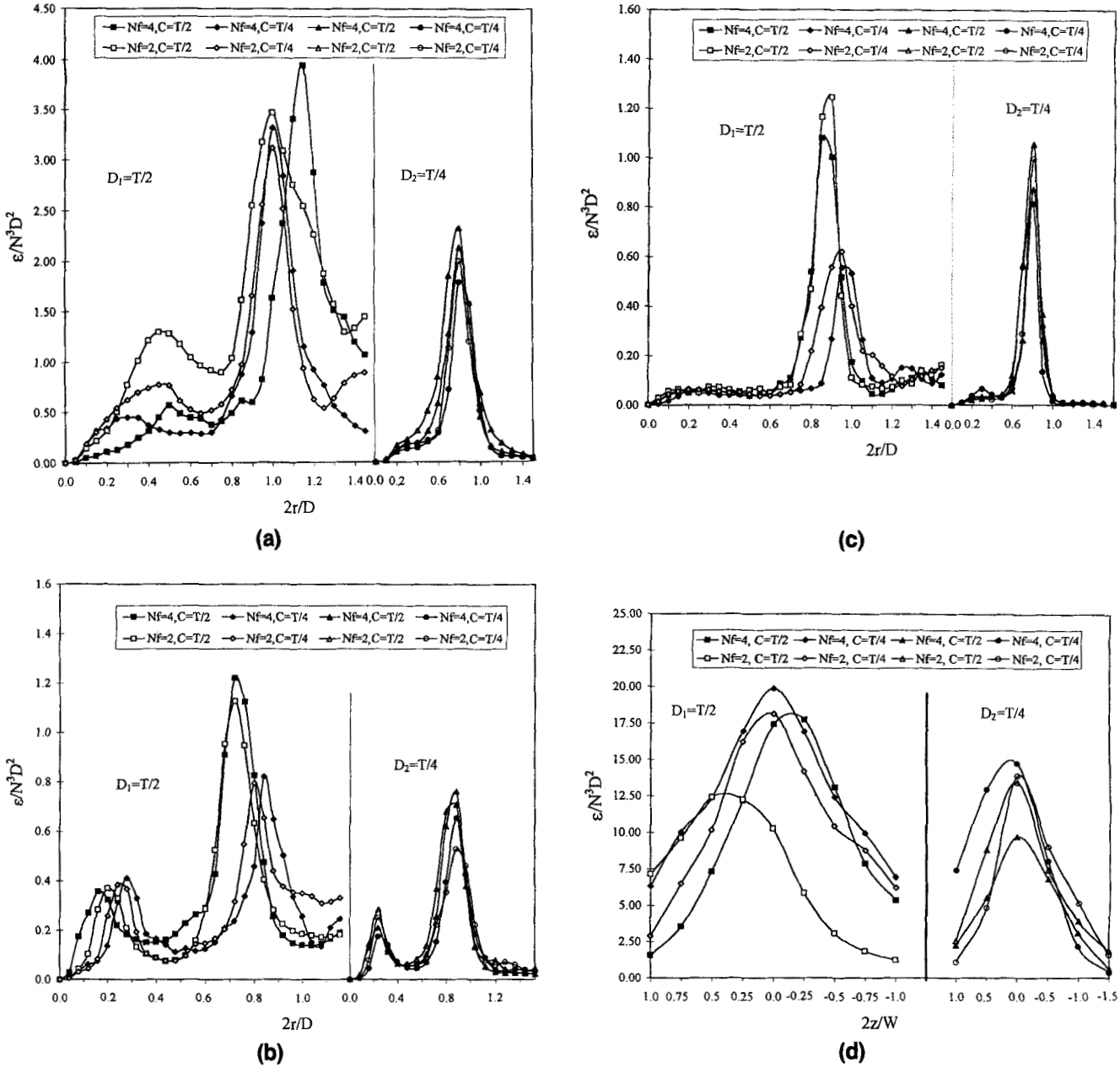


**Figure 6. Profiles of $\epsilon/N^3D^2$ showing the details of the experimental results for the factorial design based on $N_f$, $D$, and $C$.**

(a) PBT; (b) A310; (c) HE3; (d) RT.

the filled symbols used for runs with four baffles and the open symbols used for runs with two baffles. Combining analysis of the two sets of figures, the following observations are made:

1. For the PBT, the 95% confidence interval, normal probability plot, and details of the data all lead to the same conclusion; the impeller diameter is the only variable that has a significant effect on the magnitude of $\epsilon_{max}$. While the off-bottom clearance effect is slightly greater than the 95% confidence interval, it falls close to the regression line, and has a very small effect on the experimental traverses.

2. For the A310 and the HE3, the variability is much smaller, and conclusions drawn from the 95% confidence interval and the normal probability plot are less definitive. They must be combined with the experimental data before conclusions are drawn. The A310 shows a dependence on $D$ and $C$ ($\epsilon_{max}$ decreases with decreasing $C$ for both impeller diameters). The HE3 data show similar overall trends to the A310, but the significant variables are $C$ and the interaction between $C$ and $D$. Note that the $\epsilon_{max}$ values for the $D = T/4$ impeller are much larger for the HE3 (thus the lack of dependence on $D$), and that $\epsilon_{max}$ decreases with decreasing $C$ only for the $D = T/2$ impeller (leading to both the dependence on $C$ and on the interaction between $C$ and $D$).

3. Although the variation in $\epsilon_{max}$ is very large for the RT, no conclusions can be drawn from the results of this factorial design. The 95% confidence interval indicates that *all* vari-

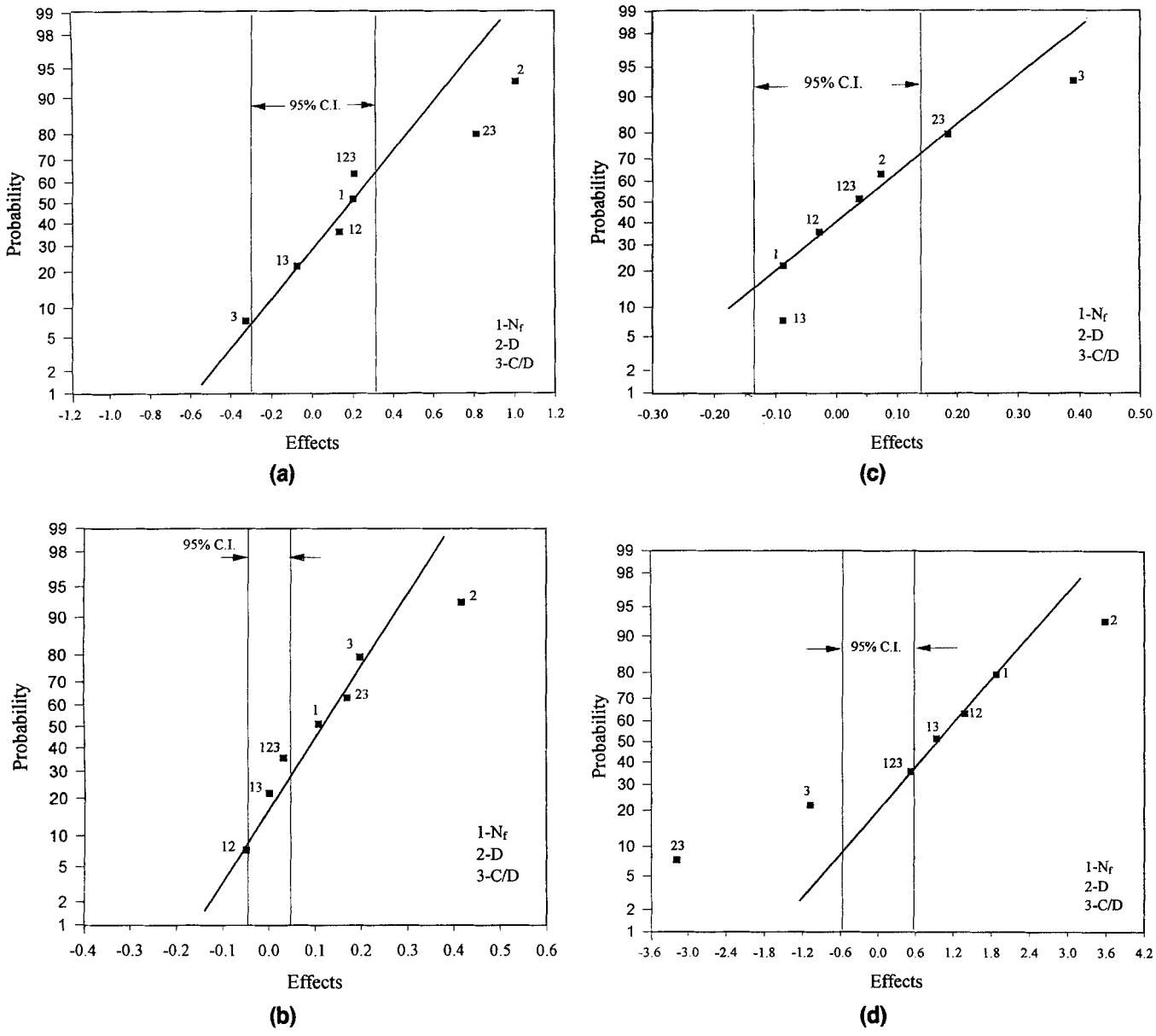


**Figure 7. Normal probability plots of the effects of geometric variables on $\epsilon_{max}/N^3D^2$ showing the 95% confidence interval around zero effect for the factorial design based on $N_f$, $D$, and $C/D$.**

(a) PBT; (b) A310; (c) HE 3; (d) RT.

ables are significant (with the exception of the interaction 13, between $N_f$ and $C$) while the normal probability plot indicates that *none* are significant, and the experimental data show no clear trends. This observation led to a reevaluation of the experimental design.

4. An overall examination of the experimental data shows clear shifts in the $D = T/2$ traverses with changes in $C$ (particularly for the A310 and HE3 impellers), while the $D = T/4$ traverses are almost identical for all three axial impellers. Kresta and Wood (1993b) reported that the flow field generated by the PBT depends on the *dimensionless* off-bottom clearance, $C/D$, not on the absolute value of $C$. A transition between two flow patterns occurs at $C/D = 0.6$. The $C/D$ values for the $D = T/2$ impeller (1.0 and 0.5) bracket this value, while the $C/D$ values for the $D = T/4$ impeller (2.0 and 1.0) are both well above the transition point. A new factorial design was implemented, which uses $C/D$ instead of $C$, with values of 1.0 and 0.5 for all impellers. This required only two additional runs for each impeller (Tables 1 to 4).

*Second Factorial Design: $N_f$, D, and C/D, Scaling Based on Constant $P/V_T$.* The 95% confidence intervals and normal probability plots for the second factorial design are shown in Figures 7a to 7d. Combining these figures with the full experimental traverses shown in Figures 8a to 8d, the following observations are made:

1. Based on an examination of the $D = T/4$ traverses in Figure 8, the change in design was justified. Distinct shifts in the position and magnitude of $\epsilon_{max}$ are now evident for the PBT, A310, and RT. For the HE3 impeller, the order and magnitude of $\epsilon_{max}$ values has changed; the decrease in $\epsilon_{max}$

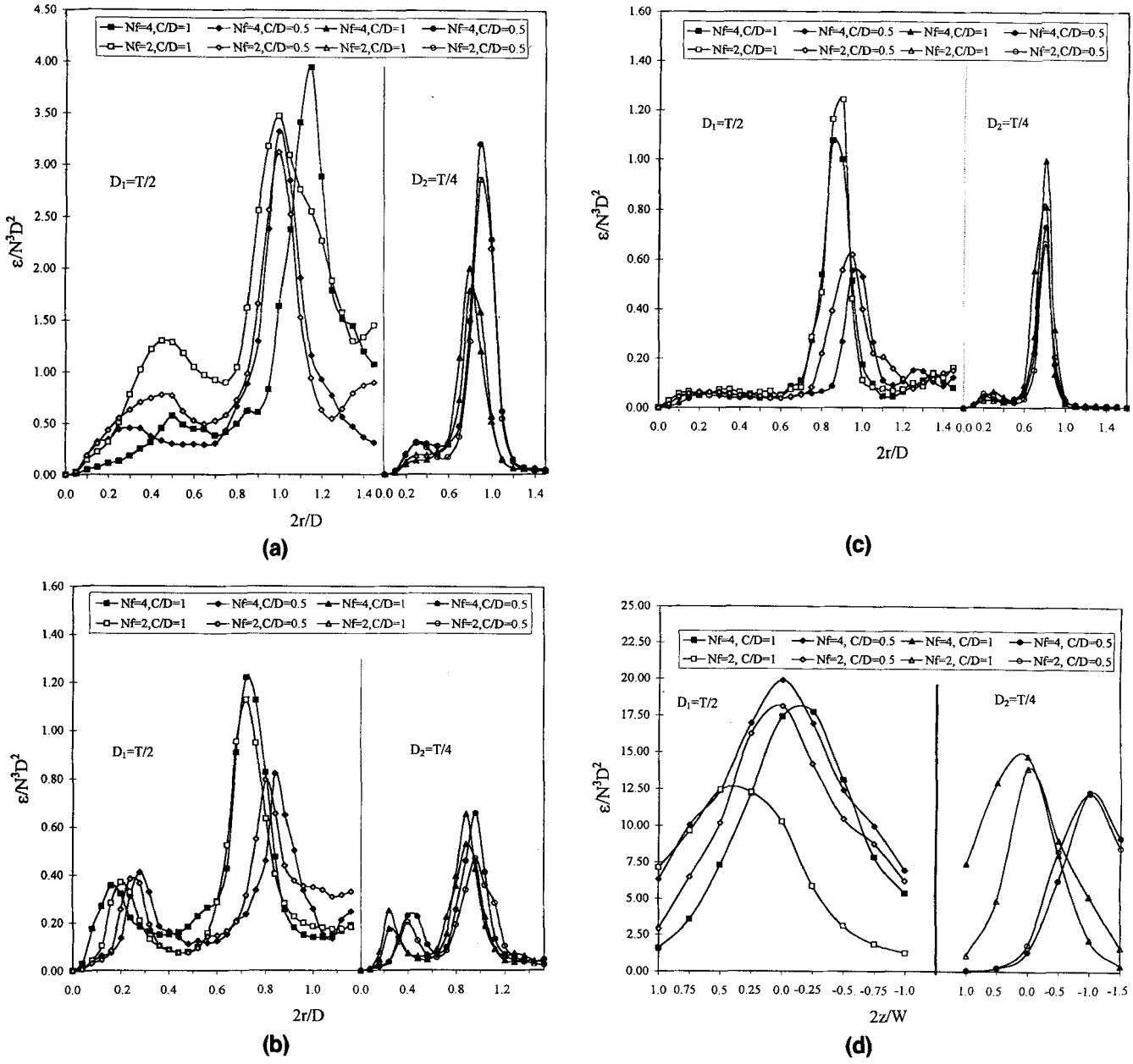


**Figure 8. Profiles of $\epsilon/N^3D^2$ showing the details of the experimental results for the factorial design based on $N_f$, $D$, and $C/D$.**

(a) PBT; (b) A310; (c) HE3; (d) RT.

with decreasing $C/D$ is roughly four times that observed with the variable $C$.

2. Returning to the analysis of individual effects, the PBT again shows the impeller diameter as the most significant effect, with the addition of the interaction between $D$ and $C/D$ (due to the additional experimental information). All three evaluation criteria (95% confidence interval, normal probability plot, and experimental traverses) are met.

3. The A310 and HE3 again show the smallest variability. Combining information from all three criteria, the impeller diameter remains the most important variable for the A310. The effect of $C/D$ is large for the $D = T/2$ impeller, but much smaller for the $D = T/4$ impeller. This gives rise to the two smaller effects of $C/D$, and the interaction of $D$ with $C/D$, both of which fall outside the 95% confidence interval, but on the regression line. Similarly, the HE3 maintains the off-bottom clearance, now in the form of $C/D$, as the largest effect. The interaction between $D$ and $C/D$ can now be neglected due to the reordering of the $D = T/4$ data as discussed previously in (1).

4. The RT results now offer some clear conclusions. The diameter is the most important variable, followed by the interaction between $D$ and $C/D$. Although the effect of $C/D$ alone falls off the regression line and is somewhat larger than the 95% confidence limit, the experimental data show that it interacts strongly with $D$ rather than providing a consistent effect when it is the only variable that is changed.

5. Both the first and second factorial designs indicate a

dependence on $D$ beyond the dependence on $D^2$ predicted by theory. This observed dependence may be due to either real interactions between the impeller and the tank walls, or due to the scaling of $N$ to maintain a constant power input (or $\bar{\epsilon}$), as opposed to scaling to maintain a constant $\epsilon$.

*Third Factorial Design: $N_f$, D, and C/D, Scaling Based on Constant $\epsilon$.* For the first two factorial designs, all rotational speeds were scaled to maintain the same power input per unit mass. Thus when the impeller diameter $D$ changed from $D_1 = T/2$ to $D_2 = T/4$, the rotational speed $N$ was changed according to the formula:

$$N_2^3 = N_1^3 \left( \frac{D_1}{D_2} \right)^5 . \tag{6}$$

When $N$ is scaled based on constant $\epsilon$, however, the rotational speed $N$ is adjusted according to:

$$N_2^3 = N_1^3 \left( \frac{D_1}{D_2} \right)^2 . \tag{7}$$

Since $\epsilon_{max} \propto N^3$ for a given impeller diameter $D$, the difference between the two methods of scaling is exactly $(D_1/D_2)^3$. In our case, $(D_1/D_2)^3$ is 8 for the PBT, HE3, and RT, and 3.88 for the A310. Dividing the $D = T/4$ results by these factors changes the scaling to a basis of constant $\epsilon$, or more specifically, $\epsilon_{max}$.

In order to compare the unscaled $\epsilon_{max}$ between the four impellers directly, the HE3 results were multiplied by a factor of 1.35 (i.e., 0.652/0.484) to correct for the smaller power input used for this impeller.

The two scaling methods are compared in Figure 9. The eight cases for each impeller are grouped into two sets of four based on impeller diameter. Runs for the RT were arranged in order of increasing $\epsilon_{max}$, and runs for the PBT, A310, and HE3 were arranged to match the RT geometry. On the right half of Figure 9, the four upper lines (solid symbols) represent the four runs scaled based on constant power input; the four lower lines (open symbols) represent the same four runs scaled for constant $\epsilon$. Scaling for constant $\epsilon$ gives much less variability in the results.

Since scaling with constant $\epsilon$ gives more constant absolute values of $\epsilon_{max}$, the factorial analysis of effects of geometry on $\epsilon_{max}$ was repeated for scaling with constant $\epsilon$. All results were adjusted as for Figure 9, and the effects recalculated.

The experimental errors were again quantified by a 95% confidence interval using the data at five different rotational speeds and the same geometry (runs $N1$ to $N5$). Because the absolute values of $\epsilon_{max}$ are used here, the $\epsilon_{max}$ values with five different rotational speeds cannot be used directly to calculate the 95% confidence interval. For the third factorial design, the $\epsilon_{max}$ at five different rotational speeds were first scaled with the appropriate value of $N^3D^2$, then multiplied by $N_1^3D_1^2$ to adjust the five $\epsilon_{max}$ to the case of $D_1 = T/2$ for the PBT, HE3, and RT or $D_1 = 0.550T$ for the A310. The calculated 95% confidence intervals for the four impellers are listed in the lower portion of Table 8.

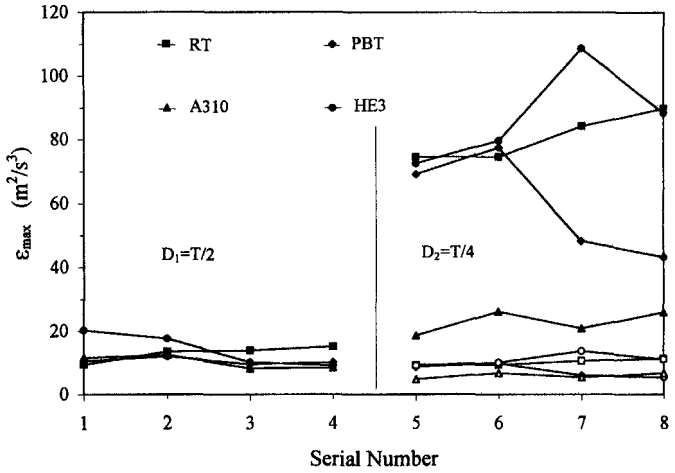


**Figure 9. Comparison of scaling based on constant power (closed symbols) vs. scaling based on constant $\epsilon_{max}$ (open symbols) when the impeller diameter is changed from $D = T/2$ to $D = T/4$.**

The resulting normal probability plots are shown in Figures 10a to 10d. From these figure parts, the following observations are made:

1. Comparison of Figures 10a to 10d with Figures 7a to 7d shows no change in the results for the PBT, A310, and RT. For these three impellers, $D$ is the dominant effect. Thus the statistical analysis of the geometric effects on the scaled $\epsilon_{max}$ for the PBT, A310, and RT based on constant power input is also true if the scaling of $N$ is based on holding $\epsilon$ constant. The effect of $D$ is due to interactions between the impeller and the tank walls, not due to the choice of scaling.

2. For the HE3, $C/D$ dominated the variation in scaled $\epsilon_{max}$ for the first two factorial designs. The normal probability plot for the HE3 shows a larger effect of $D$ and of the interaction between $D$ and $C/D$ with the rescaled data. This makes the observations for the HE3 more consistent with the observations for the other three impellers. Note that the HE3 was the only impeller for which the off-bottom clearance was the dominant effect in the first two factorial designs.

## Summary

Three forms of factorial design have been used to evaluate the effect of tank geometry on the maximum dissipation, $\epsilon_{max}$. The first design used the variables $N_f$, $D$, and $C$, but gave unclear results for the RT. Since previous investigations showed that the flow field depends on the ratio $C/D$ for the PBT, the experimental design was modified to use the variables $N_f$, $D$, and $C/D$. This second factorial design provided better results for all four impellers. Finally, in the third factorial design, the results were rescaled to a basis of constant $\epsilon_{max}$ (instead of constant power input) to verify the conclusions. Three criteria were used throughout to evaluate the significance of each geometric variable: the 95% confidence interval, a normal probability plot, and detailed examination of the experimental traverses. Taking the results of all three factorial designs together, several important conclusions can be drawn about the effect of tank geometry on $\epsilon_{max}$:

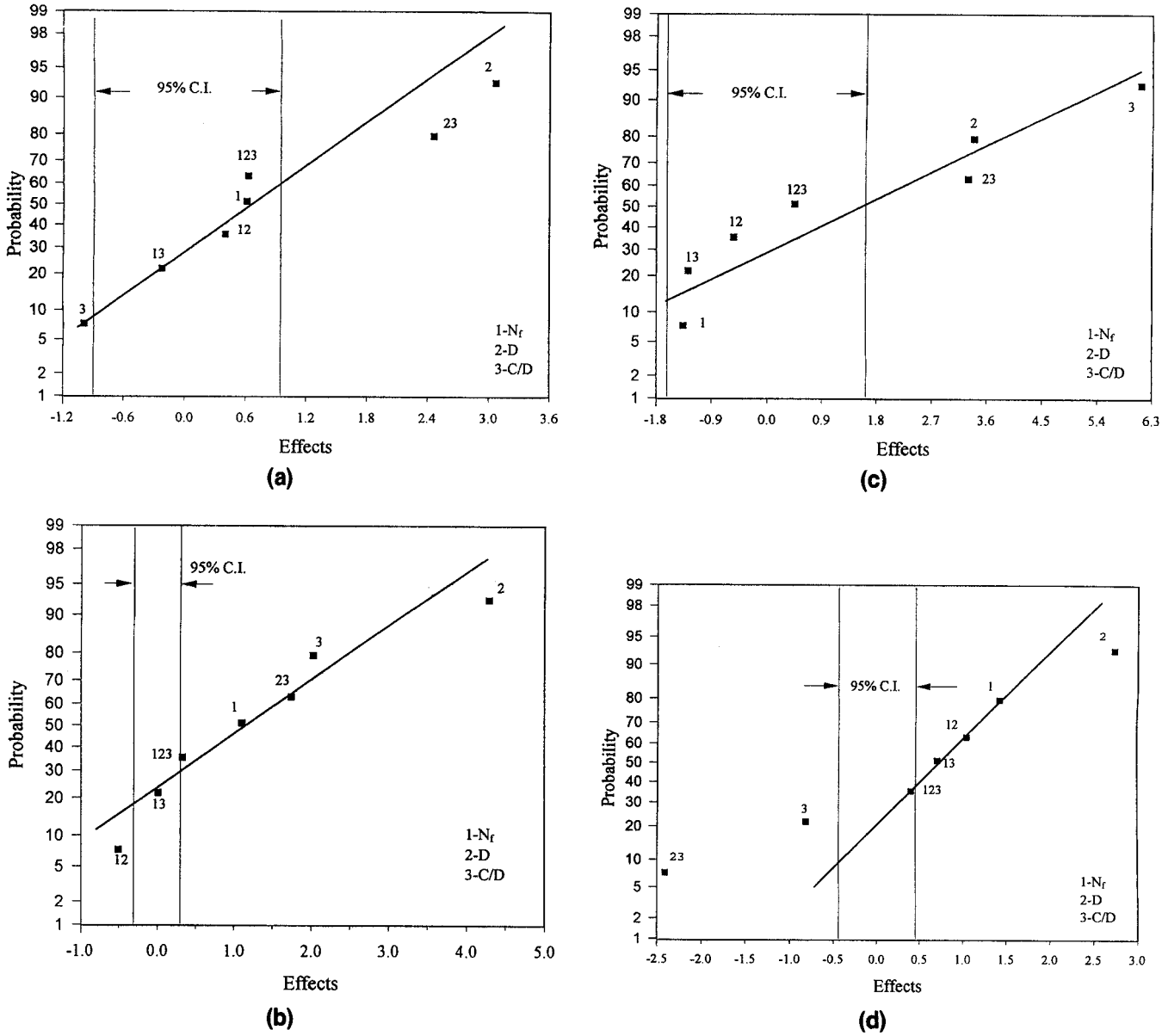


**Figure 10. Normal probability plots of the effects of geometric variables on $\epsilon_{max}$ showing the 95% confidence interval around zero effect for the factorial design based on $N_f$, $D$, and $C/D$.**

(a) PBT; $\epsilon_{max}$ for the four cases with $D = T/4$ were divided by 8. (b) A310; $\epsilon_{max}$ for the four cases with $D = 0.375T$ were divided by 3.88. (c) HE3; $\epsilon_{max}$ for the four cases with $D = T/4$ were divided by 8. (d) RT; $\epsilon_{max}$ for the four cases with $D = T/4$ were divided by 8.

1. The effect of impeller diameter on $\epsilon_{max}$ is larger than the scaling with $D^2$ predicted by theory. This can only be due to interactions between the impeller and the tank walls; put another way, significant changes in the turbulent flow field occur when the $D/T$ ratio is changed.

2. The off-bottom clearance is also an important variable, which is best quantified by its *dimensionless* form, $C/D$. It may appear as an independent variable, or in the form of interactions with the impeller diameter, depending on the impeller used. This means that *the off-bottom clearance and impeller diameter cannot be independently considered.*

3. The number of baffles, $N_f$, has no significant effect on $\epsilon_{max}$, either as an independent variable, or in the form of interactions with other geometric variables. This is true for all four impellers, and all three factorial designs.

4. To maintain a roughly constant $\epsilon_{max}$, scale-up, which is not geometrically exact, should be based on $D^2$, not on $D^5$. This is the scaling predicted from theory, not constant $P/V_T$ (equivalently constant power per unit mass, or average dissipation), which is commonly used in the literature.

## Conclusions

This article represents the first extensive analysis of the effect of tank geometry on the maximum rate of dissipation of turbulence kinetic energy, $\epsilon_{max}$. Three axial impellers (the PBT, A310, and HE3) and one radial impeller (the RT) were studied. These impellers represent the full spectrum of impellers currently used for turbulent mixing in industry. Three

geometric variables were considered: the number of baffles, the impeller diameter, and the impeller off-bottom clearance.

The local dissipation was estimated from the streamwise RMS velocity fluctuations using $\epsilon = A(v^3/L)$, where $A = 1.0$ and $L = D/10$ for all four impellers. The dissipation was shown to scale exactly with $N^3$ for the case where the tank geometry is held constant. The maximum dissipation was located on the traverse immediately below the impeller for the three axial impellers, and on the traverse at the tip of the impeller blades for the RT.

Comparison of the scaled $\epsilon_{max}$ values for all geometries considered shows significant variation between the results both when constant power input per unit volume ($P/V_T$) is used as the scaling criterion, and when $\epsilon_{max}$ is scaled with $N^3D^2$. The dominant variable was shown to be the impeller diameter. This effect is in addition to the expected scaling with $D^2$. Substantial dependence on the off-bottom clearance was also demonstrated. This dependence can be most accurately observed when the dimensionless clearance, $C/D$, is used as the experimental variable. The off-bottom clearance often interacts strongly with the impeller diameter, and thus should not be considered as an independent variable. The number of baffles had no significant effect on the $\epsilon_{max}$, either as an independent variable, or in interactions with other geometric variables. The same effects of geometric variables were observed when the results were rescaled based on maintaining a constant dissipation.

The results of this work show that the maximum local dissipation is larger for impellers with a larger power number. In addition to the dependence on power number, there is a substantial effect of tank geometry on the value of $\epsilon_{max}$. In future, experimental work that depends on $\epsilon_{max}$ should be designed to examine the effects of $D/T$, $C/D$, and interactions between the two variables on the results. Scale-up of stirred tanks should consider $\epsilon_{max}$ as well as $P/V_T$, particularly in cases where the type of impeller and/or the tank geometry are to be changed. The results contained in this work provide some guidance as to when these effects will be most important, and what values of $\epsilon_{max}$ can be expected for some standard impellers and tank configurations.

## Acknowledgment

The financial support provided by Syncrude Canada Ltd., and by NSERC, is gratefully acknowledged.

## Notation

$e_i$ = effect $i$
$P$ = power transferred to the fluid in the tank by an impeller, kg m$^2$/s$^3$
$Re$ = Reynolds number, $ND^2/\nu$
$\overline{V}_r$, $\overline{V}_z$, $\overline{V}_\theta$ = radial, axial, and tangential mean velocities, respectively, m/s
$v'_r$, $v'_z$, $v'_\theta$ = radial, axial, and tangential turbulent fluctuations, respectively, m/s
$v_\theta$ = tangential RMS velocity, m/s
$V_T$ = volume of fluid in the tank, m$^3$
$\nu$ = kinematic viscosity, m$^2$/s
$\rho$ = fluid density, kg/m$^3$

### *Subscript*

$\theta$ = tangential direction

## Literature Cited

Box, G. E. P., W. G. Hunter, and J. S. Hunter, *Statistics for Experimenters: An Introduction to Design, Data Analysis, and Model Building*, Wiley, New York, p. 306 (1978).

Costes, J., and J. P. Couderc, "Influence of the Size of the Units—II. Spectral Analysis and Scales of Turbulence," *Chem. Eng. Sci.*, **43**, 2765 (1988).

Cutter, L. A., "Flow and Turbulence in a Stirred Tank," *AIChE J.*, **12**, 35 (1966).

Kresta, S. M., and P. E. Wood, "Prediction of the Three-Dimensional Turbulent Flow in Stirred Tank," *AIChE J.*, **37**, 448 (1991).

Kresta, S. M., and P. E. Wood, "The Flow Field Produced by a Pitched Blade Turbine: Characterization of the Turbulence and Estimation of the Dissipation Rate," *Chem. Eng. Sci.*, **48**, 1761 (1993a).

Kresta, S. M., and P. E. Wood, "The Mean Flow Field Produced by a 45-degree Pitched Blade Turbine: Changes in the Circulation Pattern Due to Off Bottom Clearance," *Can. J. Chem. Eng.*, **71**, 42 (1993b).

Okamoto, Y., M. Nishikawa, and K. Hashimoto, "Energy Dissipation Rate Distribution in Mixing Vessels and Its Effects on Liquid-Liquid Dispersion and Solid-Liquid Mass Transfer," *Int. Chem. Eng.*, **21**, 88 (1981).

Wu, H., and G. K. Patterson, "Laser Doppler Measurements of Turbulent-Flow Parameters in a Stirred Mixer," *Chem. Eng. Sci.*, **44**, 2207 (1989).

Zhou, G., and S. M. Kresta, "Distribution of Energy Between Convective and Turbulent Flow for Three Frequently Used Impellers," *Trans. Ind. Chem. Eng.*, **74**, 379 (1996).

*Manuscript received Sept. 14, 1995, and revision received Jan. 2, 1996.*